Development of Human Interleukin-6 electrochemical Immunosensor Based on Pt-Pd Nanocomposite for Evaluation of Intervertebral Disc Degeneration

Fan Ding[1] and Xia Li[2,]*

[1] Department of Orthopaedic Surgery, The First People's Hospital of Jingmen , Jingmen, Hubei, 448000, P.R. China
[2] Department of Ophthalmology, The First People's Hospital of Jingmen, Jingmen, Hubei, 448000, P.R. China
*E-mail: xiali_jingmen@foxmail.com

To detect interleukin-6 (IL-6) antigen, a simple immunosensor with ultra-sensitivity was prepared. A wide linear response to IL-6 was observed with the immunosensor in range of 0.1-200 pg/mL, where the limit of detection was 0.032 pg/mL. The method described in this work, which exhibited remarkable accuracy, excellent reproducibility, comparable stability and wide linear range, can be employed to detect IL-6 in practical specimens, where these were promising in the field of evaluating intervertebral disc degeneration.

1. INTRODUCTION

An isolated native cell population regulates the tissue homeostasis in the mature intervertebral disc (IVD) [1, 2]. A continuous remodeling of tissue takes place during the generation of collagen and proteoglycan, which is in balance with the degradation of enzymatic extracellular matrix (ECM) [3, 4]. The ECM degrading enzymes generated by the native IVD cell population accelerate the degradation, of which two classes have been recognized including the matrix metalloproteinases (MMPs) and the adisintegrin metalloproteinase with thrombospondin motifs (ADAMTS) [5-9].

IVD cells, which act as an adaptive response to the changes occurring in the tissue microenvironment, regulate the ECM remodeling. The process was modulated to keep the function integrity of the tissue structures by several biochemical factors, including oxygen, mechanical stimuli, substrates and products of anaerobic metabolism [10-14].

The dysregulated ECM remodeling is employed to characterize the IVD degeneration. The rates of the ECM degradation increase when the ECM synthesis decreases, which induce the functional failure and dehydration of the degenerated IVDs [15, 16]. Numerous pro-inflammatory cytokines have been found to be involved in regulating ECM remodeling. During the degeneration of IVD, Interleukin-6 increases, which results in the ECM degradation of enzymes and decreasing the synthesis of ECM constituents *in vitro* [17-20].

Due to the highly selective and sensitive interactions between antigen (Ag) and antibody (Ab), remarkable potential applications are exhibited in immunosensing. Recently, a variety of approaches have been developed to construct interleukin immunosensors, which exhibit high selectivity and sensitivity as well as excellent limit of detection [21-26].

An amperometric immunosensor with high sensitivity for the detection of IL-6 was constructed by Wang et al. with polydopamine, which exhibits a linear response to IL-6 in the concentration range of 4.0 to 800 and a low detection limit of 1.0 pg/mL. [27]. The porous polyelectrolyte NPs supported by ferrocene was reported by Yang and Li for the detection of oral cancer biomarker IL-5 as a label, which exhibited remarkable reproducibility, a high sensitivity in a wide linear range of 0.002 to 20 ng/mL and a low detection limit of 1 pg/mL [28]. Moreover, a sphere hybrid material of silver NPs and hollow titanium phosphate was prepared by Peng et al. for the electrochemical detection of human IL-6 as a label, which displayed a highly sensitive response to IL-6 in a linear concentration range of 0.0005 to 10 ng/mL and a detection limit of 0.1 pg/mL [29].

The nanostructured materials are promising for catalysis and analysis. Because of their high effective surface area, regulation of local microenvironment, catalysis and mass transport, metal NPs including Au, Ag, Cu and Pt have been widely explored in recent years. Especially for Pt and Pt alloy NPs, they have been intensively studied in fabricating electrodes, which are utilized as essential catalysts for various chemical reactions such as the oxidation of methanol in fuel cells, oxygen reduction reaction and electrocatalytic oxidation of nitrite and biosensors [30-32].

Herein, palladium/platinum bimetallic nanoparticles (Pd-Pt NPs) were synthesized through a simple, controllable and green electrochemical method. In particular, this composite exhibited a synergistic effect on the characteristics of the individual compositions, which combined the beneficial biocompatibility of Pd NPs and Pt NPs. Pd-Pt NPs were employed to construct the immunosensor, which acted as a functionalized bionanolabel for the detection of IL-6, as Pd NPs was recognized as a reasonable platform material for immunosensors. This immunosensors exhibited remarkable advantages, including high sensitivity and selectivity to detect IL-6 and wide response range. Besides, desirable results were obtained for the practical specimens, which indicated that the proposed immunosensor was promising in evaluating the intervertebral disc degeneration in early stage.

2. EXPERIMENTS

2.1. Chemicals

IL-6 ELISA, IL-6 antibody and IL-6 antigen were commercially available (Beijing Biosynthesis Biotechnology CO., LTD). Dopamine, N-hydroxysuccinimide (NHS), lyophilized bovine serum albumin (BSA) (99%) and 1-ethyl-3-(3-dimethylaminopropyl) carbodiimide hydrochloride

(EDC) were purchased from Sigma−Aldrich. Hexachloropalladic (IV) acid (H_2PdCl_6), ploy(acrylic acid) (PAA) and polystyrene (PS) were bought from Shanghai Chemical Reagent Co. (Shanghai, China). Noted that the phosphate buffer saline (PBS, 10 mM) with a pH of 7.4 involved NaCl, Na_2HPO_4, KCl and KH_2PO_4 with a concentration of 136.7, 8.7, 2.7 and 1.4 mM, respectively, which was further employed to prepare the standard solution of IL-6 antigen stored at 4 ^{o}C. All the other chemicals were analytically pure and used without any further process. Moreover, all the aqueous solutions were produced with ultrapure water (Milli-Q, Millipore).

2.2. Synthesis and characterization of Pt–Pd NPs

According to a typical procedure, 0.2 mL $PdCl_2$ (25 mM) aqueous solution, 1mL K_2PtCl_4 aqueous solution and 1 mL PAH (0.5 M) were added to 7.5 mL water and the resultant mixture was stirred at 40 ^{o}C, where the molarity of PAH depended on the repeating unit. Then the pH of the mixture was tuned to 9.0. Subsequently, 0.2 $N_2H_4 \cdot H_2O$) (85%) was added to the mixture quickly and the mixture was mechanically stirred at 60 ^{o}C for 3 h. Thereafter, the as-synthesized Pd-Pt NPs were separated through centrifuging at 15000 rpm for 10 min, rinsed with water for several times and dried under vacuum at 60 ^{o}C for 5 h. At last, UV/Ozone was employed to remove the capping agent on the catalyst. Moreover, the mono-component Pt nanoflowers were synthesized as reference under the similar experimental conditions through employing K_2PtCl_4 as precursor.

2.3. Fabrication of immunosensors

A competitive immunosensors was fabricated to detect IL-6. First, the electrode, which was modified with Au-Pd NPs, was immersed in 20 □L anti-IL-6 with a concentration of 100 mg/L for 12 h. After that, the electrode was rinsed with PBS buffer in prior to be immersed in PBS solution with 3% BSA at 37 ^{o}C for 1 h, where the nonspecific binding sites as well as the excess active groups on the surface were blocked. Subsequently, the electrode was further immersed in bionanolabel with a definite concentration for 40 min. A competition for the finite binding sites to anchor anti-IL-6 on the surface of the electrode was observed between the IL-6 in the incubation solution and the bionanolabel to form immunocomplex. At last, PBS was utilized to wash the electrode thoroughly so that to remove the nonspecific-binding Ab2 conjugates. Noted that the as-prepared immunosensor should be stored at 4 ^{o}C when not in use.

2.4. Instruments

CHI 760 electrochemical workstation with an Autolab electrochemical analyzer (Eco Chemie, The Netherlands) was employed to record Electrochemical impedance spectroscopy (EIS), where the measurements were carried out in the mixture of $K_3Fe(CN)_6/K_4Fe(CN)_6$ (1:1) with a concentration of KCl (1.0 M) which acted as the supporting electrolyte. Besides, 5.0 mV alternating current voltage was employed as well as the frequency range of 0.1 to 10000 Hz. A contact angle meter (Rame-Hart-100)

was used to measure the static water contact angles with drops of pure deionized water at 25 ^{o}C. After the addition of samples, the readings were settled and recorded in 120 s. In prior to perform the electrochemical measurement, the immunosensor was immersed in 200 μL KCl with a concentration of 1.0 M, where the linear sweep voltammetry (LSV) was used to quantify the silver component which was utilized as the detector target. Especially, the heated-electrode approach was used to amplify the signal in the final stripping analysis.

3. RESULTS AND DISCUSSION

XRD and EDS were employed to analyse the structure and composition of the Pt-Pd NPs. The EDS data was shown in Figure 1A, where the atomic ration of Pt to Pd in the Pt-Pd NPs was calculated to be 3:1, which was in accordance with theoretically stoichiometric value. XRD patterns were illustrated in Figure 1B, which suggested that the structure of Pt-Pd NPs could be recognized as fcc. Besides, it was obvious that a slight shift to higher value took place in the diffraction peaks of the Pt-Pd NPs compared with the commercial Pt black, which demonstrated the formation of Pt/Pd alloy [33, 34]. According to the four diverse peaks, the mean lattice parameter value (*a*) of the Pt-Pd NPs was calculated to be 0.39150 nm, which fell in between bulk Pt and Pd samples. It indicated that the lattice contracted owing to the partial substitution of Pt by Pd. The mean content of Pd in the Pt-Pd alloy NPs was calculated to be 24.6 atom% from the four different diffraction peaks based on the Vegard's law [35, 36]. This was in accordance with the composition of bulk which was measured by EDS. As a matter of fact, the mean size of nanoparticles could be obtained according to the width of the XRD peaks. Generally, the size of nanoparticles decreases when the XRD peak becomes broader. Hence, the mean particle size (d_{XRD}) of the Pt-Pd alloywas calculated to 5.2 nm based on the Scherrer equation, which was smaller compared with the commercial Pt black (d_{XRD} = 8.4 nm). The size decreasing is not only minimizes the surface energy but also induces mechanical integrity with high Young's modulus and tensile strength, due to small nanoscale particle size [37].
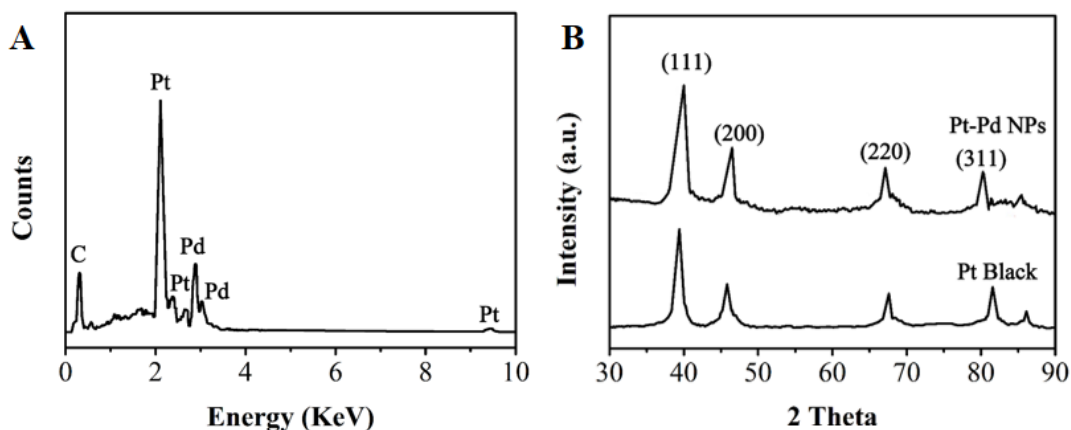

Figure 1. (A) EDS spectrum of the Pt–Pd NPs. (B) XRD patterns of the Pt–Pd NPs and commercial Pt black.

Furthermore, the surface chemical states and the composition of Pt-Pd NPs could be confirmed through XPS. The signal of Pt 4f in the Pt-Pd NPs could be deconvoluted into two constituents. In Figure 2A, the binding energies of the two pairs of the double peaks, which located at Pt 4f7/2 (71.34 eV), Pt 4f5/2 (74.65 eV), and Pt 4f7/2 (72.88 eV), Pt 4f5/2 (76.33 eV), could be ascribed to the corresponding Pt^0 and Pt^{II} species, respectively. According to the corresponding peak areas obtained through the curve-fitting, the content of Pt^0 species in the Pt–Pd NPs could be calculated to be 92.7%. Moreover, compared with the theoretical value, a negative shift of about 0.4 eV was observed in binding energy value of Pt^0 species in the Pt-Pd NPs, which was primarily due to the interaction between Pt atoms and PAH. In fact, because of the lone pair electrons in -NH2 group, the N atom of PAH exhibited a high electron density. Hence, the electrons of the N atoms could be withdrawn by the adjacent Pt, which induced the shift of the binding energies. Besides, 5d vacancies in Pt decreased due to the electron donation from N atom to Pt, resulting in the decrease of electron donation from O_2 to Pt. Hence, the adsorption of O_2 became weaker. In Figure 2B, it was obvious that remarkable Pd^0 $3d_{5/2}$ and Pd^0 $3d_{3/2}$ peaks took place in the Pd 3d region, which suggested that a thorough reduction of the Pd^{II} precursors were achieved in our synthesis. Similar results have been observed by other researchers as well [38-40].
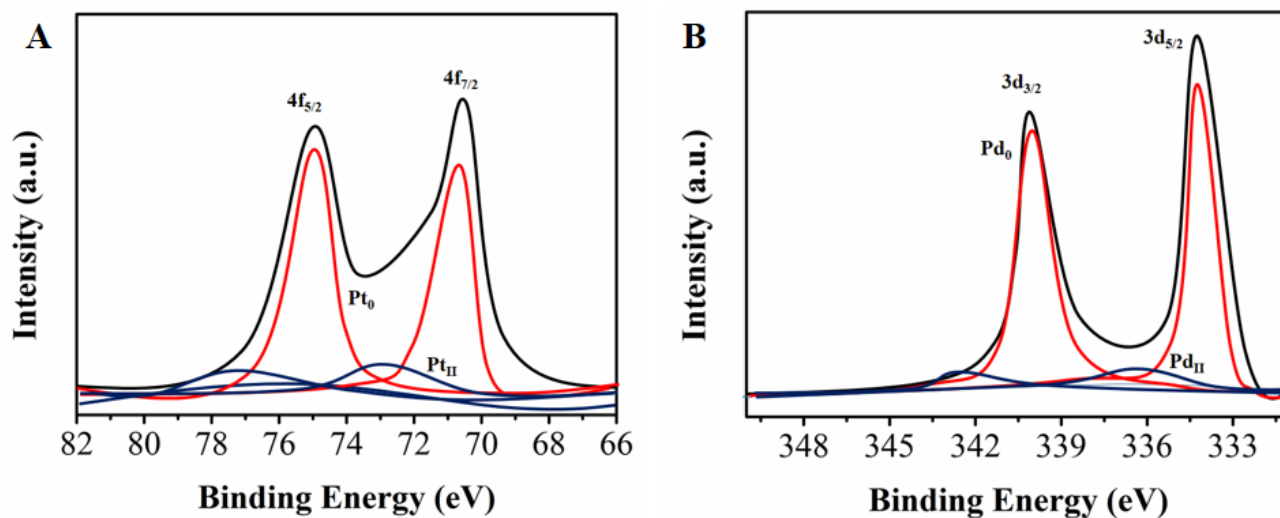

Figure 2. XPS spectra of Pd-Pt NPs in the region of Pt 4f (A) and Pd 3d (B).

EIS measurements were employed to record the change of the electrode-transfer resistance to analyze the fabrication process of immunosensor, where using $[Fe(CN)_6]^{3-}/^{4-}$ acted as the redox probe. It was obvious that the EIS curves exhibited two parts including the semicircular and the straight line. The semicircular represented the electron transfer limited process status of the electrode, where the diameter equaled to the value of the electron transfer resistance. As shown in Figure 3, the charge transfer resistance (*Rct*, the diameter of the semicircle in EIS) of Pt–Pd NPs/GCE significantly decreased compared to the bare GCE, which indicated that the film of Pt-Pd NPs accelerated the diffusion of the $K_3[Fe(CN)_6]/K_4[Fe(CN)_6]$ redox probe towards the surface of the electrode. A

consecutive increase of the resistance was observed when absorbing the anti-IL-6 and BSA/anti-IL-6 onto the surface of the Pt-Pd NPs, which could be owing to the electron transfer on the electrode inhibited by the successive modifications with the insulating proteins.
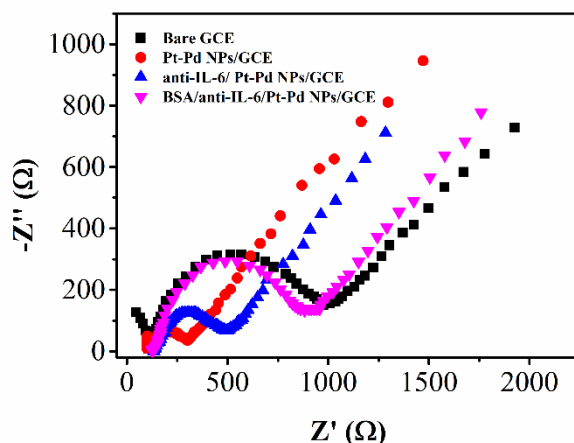

Figure 3. EIS of bare GCE, Pt–Pd NPs/GCE, anti-IL-6/ Pt–Pd NPs/GCE and BSA/anti-IL-6/Pt–Pd NPs/GCE in $[Fe(CN)_6]^{3-/4-}$ with a concentration of 10 mM in the presence of 0.1 M KCl.

In general, the analytical performance of the immunosensor reported in this work was influenced by the conjugating reaction time of the antigen and antibody as well as the concentration of IL-6. In Figure 4A, an increasing response was observed in the peak current when the concentration of IL-6 increased until the volume of IL-6 reached up to 10 µL, which indicated that all the recognition sites available to immobilize anti-IL-6 were suitable for the nanoprobe. Hence, the optimized amount of IL-6 was selected to be 10 µL. In Figure 4B, the peak current changed when the immersion time varied ranging from 10 to 70 min at the optimum concentration, which would reach to the maximum at the immersion time of 40 min. This might be owing to that the target protein thoroughly covered the surface.
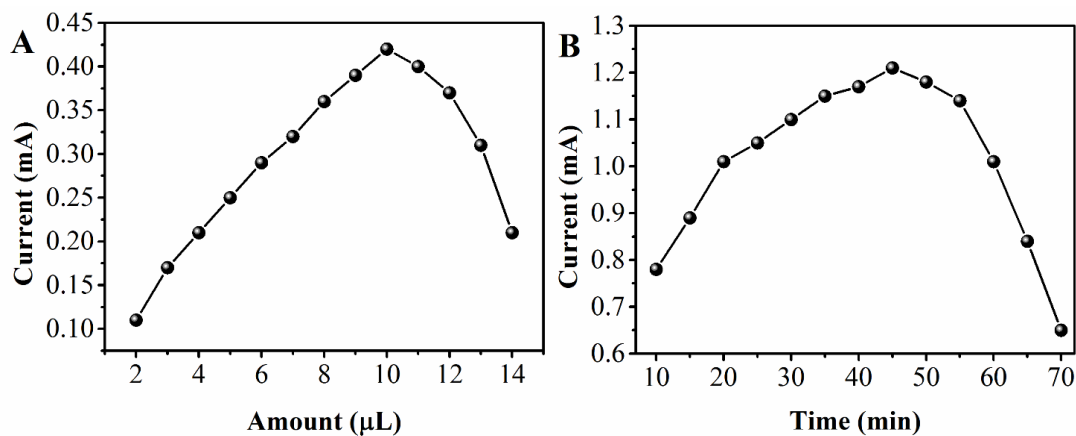

Figure 4. The influences of the concentration of IL-6 (A) and the incubation time (B) on the peak currents of LSV at BSA/anti-IL-6/Pt–Pd NPs/GCE.

However, the current decreased when prolonging the immersion time, which could be induced by the deactivation of the protein. Hence, 45 min was considered as the optimum immersion time to detect the target protein adequately.The measurements of the routine samples with IL-6 in various concentrations were performed at 25 ^{o}C to analyze the quantitative and sensitive response range of the designed immunosensors, where the competitive-type immunosensor based on BSA/anti-IL-6/Pt-NPs/GCE was employed. In Figure 5A, the LSV peak current of the immunosensor decreased when the concentration of IL-6 in the incubation solution increased. In Figure 5B, a remarkable linear relationship was observed between the semi-log of the peak current and the concentration of IL-6 in the range of 0.1-2000 pg/mL, where the LOD was found to be 0.032 pg/mL when the ratio of signal to noise reached to 3. Besides, the carbon paste electrode (CPE) was utilized as reference to record the amperometric response of the designed immunosensor at 25 ^{o}C. Nevertheless, the linear relationship could only be obtained in a relatively narrow concentraion range from 10 to 1000 pg/mL, where the LOD was 4.41 pg/mL. The sensitivity of the BSA/anti-IL-6/Pt–Pd NPs/GCE was compared with that of other reported modified electrodes and the results were presented in Table 1. This low detection limits might be attributed to the enormous loading of Pt-Pd NPs which greatly amplified the stripping peak signals.
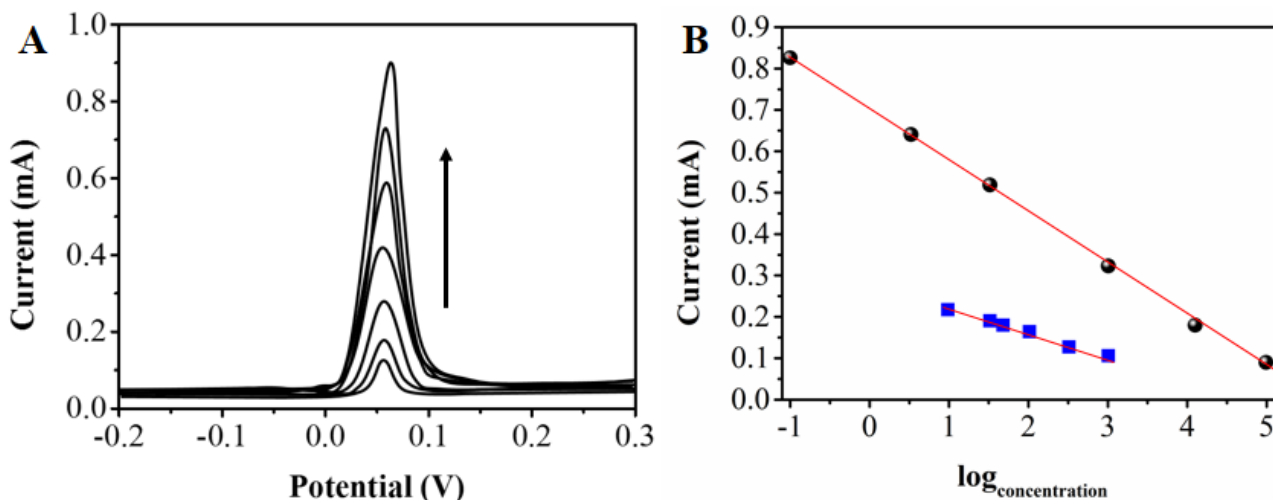

Figure 5. (A) Characteristic LSV responses of the immunosensor to IL-6 with a concentration in the range of 0.1 to 2000 pg/mL, which were collected on BSA/anti-IL-6/Pt–Pd NPs/GCE at 25 °C. (B) The resultant calibration curves of IL-6 were plotted on a semi-log scale, where the black line and red line were both heated at 25°C.

Table 1. Comparison of the present BSA/anti-IL-6/Pt–Pd NPs/GCE with other IL-6 determination methods.

Electrode	Linear detection range	Detection limit	Reference
CuInS$_2$/ZnS Nanocrystals	0.02-20 ng/mL	0.008 ng/mL	[41]
TiO$_2$/CdS/CdSe	1-30000 pg/mL	0.38 pg/mL	[42]
ELISA	1-100 pg/mL	1 pg/mL	[43]
BSA/anti-IL-6/Pt–Pd NPs/GCE	0.1-2000 pg/mL	0.032 pg/mL	This work

In addition, IL-6 with a concentration of 10 pg/mL was mixed with hum BSA, carcinoembryonic antigen (CEA), cardiac troponin I (cTnI) and matrix metalloproteinase-2 (MMP-2) with the same concentration respectively so that to evaluate the specificity of the designed immunosensor. In Figure 6A, no obvious changes (R.S.D in the range of 6.2 to 11.5%) were observed with these samples compared with the response of immunosensor in the presence of pure IL-6 with a concentration of 10 pg/mL, which suggested that the interferences of the BSA, CEA, cTnI and MMP-2 were negligible. Besides, the response of the immunosensor to IL-6 remained higher than 93% of the original one when it was placed at 4 ^{o}C for 2 weeks. It indicated that the immunosensor exhibited a remarkable stability, which could be owing to the excellent biocompatibility of Pt-Pd NPs retaining the bioactivity of the proteins. However, because of the progressive deactivation of the anchored biomolecules, the responses decreased slightly. Moreover, the proposed immunosensor was tested with the patient serum samples compared with ELISA technique, so that to evaluate the analytical reliability and the potential application. Figure 6B illustrated the results, which indicated that the proposed immunosensor exhibited a remarkable performance compared to ELISA approach, where an acceptable result below 4.6% was obtained with RSD. Hence, the proposed immunosensor was feasible for evaluating the intervertebral disc degeneration in early state.
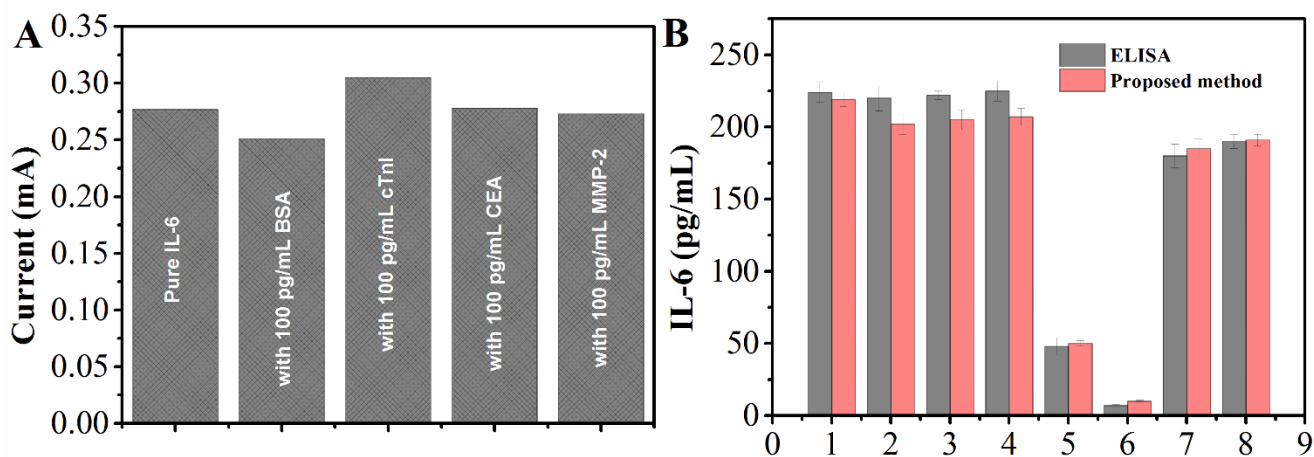

Figure 6. (A) The specificity of the immunosensor to IL-6 in other protein with a concentration of 10 pg/mL. (B) Comparison of the determination levels of IL-6 in serum through electrochemical immunoassay and ELISA approach.

4. CONCLUSIONS

In conclusion, we synthesized the Pd-Pt NPs through a simple one-pot chemical reduction approach, which was performed in a PAH-based aqueous system. Especially, the Pd-Pt NPs exhibited a high shape selectivity. Then, a novel electrochemical immunosensor was constructed to detect human IL-6 by employing the Pd-Pt NPs/GCE as platform. The obtained immunosensor displayed a comparable stability, excellent reproducibility and broad linear response in range of 0.1 to 2000 pg/mL, where the limit of detection was 0.032 pg/mL. Moreover, desirable results were observed in

detecting IL-6 in serum specimens. Hence, this dual signal amplification approach exhibited remarkable performance towards the detection of IL-6, which indicated it was promising in early-evaluating intervertebral disc degeneration.

References

1. M.K. Chelberg, G.M. Banks, D.F. Geiger and T.R. Oegema Jr, *Journal of anatomy*, 186 (1995) 43
2. T. Liebscher, M. Haefeli, K. Wuertz, A.G. Nerlich and N. Boos, *Spine*, 36 (2011) 153
3. J. Antoniou, N.M. Goudsouzian, T.F. Heathfield, N. Winterbottom, T. Steffen, A.R. Poole, M. Aebi and M. Alini, *Spine*, 21 (1996) 1153
4. J. Antoniou, T. Steffen, F. Nelson, N. Winterbottom, A.P. Hollander, R.A. Poole, M. Aebi and M. Alini, *Journal of Clinical Investigation*, 98 (1996) 996
5. J.K. Crean, S. Roberts, D.C. Jaffray, S.M. Eisenstein and V.C. Duance, *Spine*, 22 (1997) 2877
6. O. Nemoto, M. Yamagishi, H. Yamada, T. Kikuchi and H. Takaishi, *Clinical Spine Surgery*, 10 (1997) 493
7. S. Roberts, B. Caterson, J. Menage, E.H. Evans, D.C. Jaffray and S.M. Eisenstein, *Spine*, 25 (2000) 3005
8. A.J. Pockert, S.M. Richardson, C.L. Le Maitre, M. Lyon, J.A. Deakin, D.J. Buttle, A.J. Freemont and J.A. Hoyland, *Arthritis & Rheumatism*, 60 (2009) 482
9. E. Hatano, T. Fujita, Y. Ueda, T. Okuda, S. Katsuda, Y. Okada and T. Matsumoto, *Spine*, 31 (2006) 1426
10. C. Bonnans, J. Chou and Z. Werb, *Nature reviews Molecular cell biology*, 15 (2014) 786
11. D.M. Gilkes, G.L. Semenza and D. Wirtz, *Nature Reviews Cancer*, 14 (2014) 430
12. F. Mercier, *Cellular and Molecular Life Sciences*, (2016) 1
13. B. Markway, H. Cho, D. Anderson, P. Holden, V. Ravi, C. Little and B. Johnstone, *Eur Cell Mater*, 31 (2016) 425
14. E. Elagamey, K. Narula, A. Sinha, P.R. Aggarwal, S. Ghosh, N. Chakraborty and S. Chakraborty, *Proteomes*, 4 (2016) 20
15. J. Urban and J. McMullin, *Spine*, 13 (1988) 179
16. K.H. Wenger, J.A. Woods, A. Holecek, E.C. Eckstein, J.T. Robertson and K.A. Hasty, *Spine*, 30 (2005) 1122
17. C. Weiler, A.G. Nerlich, B.E. Bachmeier and N. Boos, *Spine*, 30 (2005) 44
18. B.E. Bachmeier, A.G. Nerlich, C. Weiler, G. PAESOLD, M. Jochum and N. Boos, *Annals of the New York Academy of Sciences*, 1096 (2007) 44
19. C.L. Le Maitre, J.A. Hoyland and A.J. Freemont, *Arthritis research & therapy*, 9 (2007) 1
20. S.J. Millward-Sadler, P.W. Costello, A.J. Freemont and J.A. Hoyland, *Arthritis research & therapy*, 11 (2009) 1
21. R. Torrente-Rodríguez, S. Campuzano, V.R.-V. Montiel, M. Gamella and J. Pingarrón, *Biosensors and Bioelectronics*, 77 (2016) 543
22. Y. Yan, S. Shi, J. Yu, M. Zhang, Y. Zhang, H. Huang, J. Li and Z. Jiang, *Int. J. Electrochem. Sc.*, 10 (2015) 6475
23. E. Alipour, H. Shahabi and T. Mahmoudi-Badiki, *Journal of Solid State Electrochemistry*, (2016) 1
24. P. Tang, H. Zhang, J. Huo and X. Lin, *Analytical Methods*, 7 (2015) 7784
25. F. Ding, Z.-W. Shao, S.-H. Yang, Q. Wu, F. Gao and L.-M. Xiong, *Apoptosis*, 17 (2012) 579
26. F. Ding, Z.-w. Shao and L.-m. Xiong, *Apoptosis*, 18 (2013) 777
27. G. Wang, H. Huang, G. Zhang, X. Zhang, B. Fang and L. Wang, *Langmuir*, 27 (2010) 1224
28. T. Li and M. Yang, *Sensors and Actuators B: Chemical*, 158 (2011) 361
29. J. Peng, L.N. Feng, Z.J. Ren, L.P. Jiang and J.J. Zhu, *Small*, 7 (2011) 2921
30. H.-F. Cui, J.-S. Ye, W.-D. Zhang, J. Wang and F.-S. Sheu, *Journal of Electroanalytical Chemistry*,

577 (2005) 295
31. X. Niu, M. Lan, C. Chen and H. Zhao, *Talanta*, 99 (2012) 1062
32. Y. Li, X. Niu, J. Tang, M. Lan and H. Zhao, *Electrochimica acta*, 130 (2014) 1
33. K. Nishanth, P. Sridhar, S. Pitchumani and A. Shukla, *Journal of The Electrochemical Society*, 158 (2011) B871
34. D. Hotza and J.D. da Costa, *International Journal of Hydrogen Energy*, 33 (2008) 4915
35. S.I. Lim, M. Varón, I. Ojea-Jiménez, J. Arbiol and V. Puntes, *Chemistry of Materials*, 22 (2010) 4495
36. C.-T. Hsieh, J.-L. Wei, J.-Y. Lin and B.-H. Yang, *Diamond and Related Materials*, 20 (2011) 1065
37. Y. Xu, H. Bai, G. Lu, C. Li and G. Shi, *Journal of the American Chemical Society*, 130 (2008) 5856
38. E. Asadian, S. Shahrokhian, A. Iraji Zad and F. Ghorbani-Bidkorbeh, *Sensors and Actuators B: Chemical*, 239 (2017) 617
39. P. Lv, X.-W. Tan, K.-H. Yu, R.-L. Zheng, J.-J. Zheng and W. Wei, *Carbon*, 99 (2016) 222
40. J. Zhao, Y. Liu, X. Quan, S. Chen, H. Zhao and H. Yu, *Electrochimica Acta*, 204 (2016) 169
41. W.-W. Xiong, G.-H. Yang, X.-C. Wu and J.-J. Zhu, *ACS applied materials & interfaces*, 5 (2013) 8210
42. G.-C. Fan, X.-L. Ren, C. Zhu, J.-R. Zhang and J.-J. Zhu, *Biosensors and Bioelectronics*, 59 (2014) 45
43. M. Helle, L. Boeije, E. de Groot, A. de Vos and L. Aarden, *Journal of Immunological Methods*, 138 (1991) 47